HHS Public Access

Author manuscript

J Thromb Haemost. Author manuscript; available in PMC 2024 January 17.

Published in final edited form as:

J Thromb Haemost. 2023 September ; 21(9): 2390–2404. doi:10.1016/j.jtha.2023.04.022.

Maladaptive lymphangiogenesis is associated with synovial iron accumulation and delayed Clearance in FVIII$^{-/-}$ mice after induced hemarthrosis

Esther J Cooke[1,*], **Bilgimol C Joseph**[1,*], **Chanond A Nasamran**[2], **Kathleen M Fisch**[2], **Annette von Drygalski**[1]

[1]University of California San Diego, Department of Medicine, Division of Hematology/Oncology, La Jolla, CA, USA

[2]University of California San Diego, Center for Computational Biology and Bioinformatics, La Jolla, CA, USA

Abstract

Background: Mechanisms of iron clearance from hemophilic joints are unknown.

Objectives: To better understand mechanisms of iron clearance following joint bleeding in a mouse model of hemophilia.

Methods: Hemarthrosis was induced by subpatellar puncture in FVIII$^{-/-}$ mice, +/− peri-procedural recombinant human FVIII (rhFVIII), and in hypocoagulable (^{Hypo}BALB/c) mice. ^{Hypo}BALB/c mice experienced transient FVIII-deficiency (anti-FVIII antibody) at the time of injury combined with warfarin-induced hypocoagulability. Synovial tissue was harvested weekly up to 6 weeks after injury for histological analysis, ferric iron and macrophage accumulation (CD68), blood and lymphatic vessel remodeling (αSMA; LYVE1). Synovial RNA sequencing was performed for FVIII$^{-/-}$ mice at Days 0, 3 and 14 after injury to quantify expression changes of iron regulators and lymphatic markers.

Results: Bleed volumes were similar in FVIII$^{-/-}$ and ^{Hypo}BALB/c mice. However, pronounced and prolonged synovial iron accumulation co-localizing with macrophages, and impaired lymphangiogenesis were only detected in FVIII$^{-/-}$ mice and were prevented by peri-procedural FVIII. Gene expression changes involved in iron handling (some genes with dual roles in

Corresponding Author: Annette von Drygalski, MD, PharmD, Hemophilia and Thrombosis Treatment Center, University of California San Diego, Department of Medicine, Division of Hematology/Oncology, 9333 Genesee Avenue Suite 310, La Jolla, CA 92121. Ph. +1 858-657-6028, avondrygalski@health.ucsd.edu.

Addendum

EJC and BCJ performed the experimental work and contributed to data analysis and interpretation. EJC provided the first draft of the manuscript, BCJ contributed to manuscript drafting. CAN and KMF performed primary RNAseq analyses. AvD provided concept and study oversight, contributed to data analysis and interpretation, and contributed to manuscript drafting.

*Equal Contributions

Conflicts of Interest

AvD has received honoraria for participating in scientific advisory board panels, consulting, and speaking engagements for Biomarin, Regeneron, Pfizer, Bioverativ/Sanofi, CSL-Behring, Novo Nordisk, Spark Therapeutics, Genentech and UniQure. AvD is a co-founder and member of the Board of Directors of Hematherix LLC., a biotech company that is developing ^{super}FVa therapy for bleeding complications. EJC, BCJ, KMF, and CAN have nothing to disclose.

inflammation) and lymphatic markers supported pro-inflammatory milieu with iron retention and disturbed lymphangiogenesis.

Conclusions: Accumulation and delayed clearance of iron-laden macrophages was associated with defective lymphangiogenesis after hemarthrosis in FVIII$^{-/-}$ mice. The absence of such findings in ^{Hypo}BALB/c mice suggests that intact lymphatics are required for removal of iron-laden-macrophages, and that these processes depend on FVIII availability. Studies to elucidate the biological mechanisms of disturbed lymphangiogenesis in hemophilia appear critical to develop new therapeutic targets.

Keywords

Factor VIII; Hemarthrosis; Iron; Macrophages; Lymphangiogenesis; Inflammation; Hemophilia

1 Introduction

Hemophilia A (Factor VIII [FVIII] deficiency) causes recurrent joint bleeding, which cannot be fully prevented despite improvements in prophylactic clotting factor and factorless replacement therapies [1, 2]. Hemarthroses cause a progressive arthropathy (hemophilic arthropathy [HA]), characterized by synovial inflammation and vascular remodeling, as well as osteochondral damage [3, 4].

After hemarthrosis, iron is released into the surrounding tissue by lysis of extravasated erythrocytes. Extracellular ferrous iron (Fe^{2+}) is converted to ferric iron (Fe^{3+}) for storage, causing oxidative stress and cellular injury due to formation of superoxide, hydrogen peroxide, and hydroxyl radicals [5]. Synovial ferric iron is stored as extracellular aggregates known as hemosiderin, or intracellularly in type A (macrophage-like) synoviocytes [6]. Synovial hemosiderin accumulation is widely reported in patients with hemophilia and has been ascribed a major role in creating a toxic milieu promoting joint destruction [7, 8].

Exposure of synoviocytes to iron stimulates synovial proliferation and hypertrophy via upregulation of proto-oncogenes *C-myc* and *Mdm2* [9, 10]. It also triggers the release of proinflammatory cytokines, including interleukin (IL)-1β, IL-6, and tumor necrosis factor (TNF)-α from synoviocytes and infiltrating M1 macrophages [11–14]. Additionally, iron-induced oxidative stress causes chondrocyte apoptosis and impaired osteoblast function [15], whereby cartilage iron loading has been associated with poorer clinical joint outcomes [16, 17].

We previously demonstrated in humans and mice that hemarthrosis provokes vascular changes, including neovascularization, vascular remodeling, and increased vascular permeability, which may promote rebleeding [13, 14, 18]. In mouse models synovitis and vascular changes associated with hemarthrosis were more pronounced in FVIII$^{-/-}$ mice than in ^{Hypo}BALB/c mice with similar bleed volumes [14]. In turn, this may influence prolonged iron retention in the joint since inflammation has been shown to be associated with iron retention in the reticuloendothelial system [19, 20].

Despite growing evidence that iron accumulation contributes to the progression of HA, which includes studies related to the usefulness of iron chelators in HA [21, 22], the processes involved in trafficking excess iron out of the joint tissue have not been described. This study aimed to examine the extent and duration of synovial iron accumulation after hemarthrosis, with a comparison of responses in FVIII$^{-/-}$ mice (+/−rhFVIII) and ^{Hypo}BALB/c mice. Further, we explored mechanisms of iron clearance by examining gene expression changes, tissue hypertrophy, macrophage infiltration, and vascular remodeling in relation to synovial iron levels. This included visualization of lymphatic vessel remodeling, which has not previously been studied in HA.

2 Materials and Methods

2.1 Mice

FVIII-deficient (FVIII$^{-/-}$) mice on a BALB/c background were provided by Prof. David Lillicrap (Queen's University, Kingston, ON) [23] and BALB/cByJ mice were purchased from Jackson Laboratories (Bar Harbor, ME). In-house breeding colonies were established, and housing conditions and experiments were in accordance with guidelines and protocols approved by the Institutional Animal Care and Use Committee at the University of California San Diego (UCSD).

2.2 Knee injury to induce hemarthrosis in FVIII$^{-/-}$ mice

Skeletally mature (12–16 weeks old) FVIII$^{-/-}$ mice of both genders were used to induce hemarthrosis by 4 subpatellar punctures of the right knee with a 30-gauge needle. The extent of intra-/peri-articular bleeding was inferred in all mice by determination of a spun hematocrit on Day 2 after injury [13, 14, 18]. A subset of FVIII$^{-/-}$ mice were treated with 100 IU/kg recombinant human FVIII (rhFVIII) prophylaxis given intravenously 2 hours before knee puncture, with a second dose 6 hours later ("peri-procedural" rhFVIII administration). The 100 IU/kg dose effectively reduces joint bleeding after knee injury [14, 24]. All other mice were administered an equivalent volume of saline (vehicle control) by intravenous injection. Joint tissue was harvested at baseline and Day 3, 2 weeks, 4 weeks, or 6 weeks after injury for histology. Synovial tissue was harvested at baseline, Day 3, and 2 weeks after injury for RNA sequencing.

2.3 Knee injury to induce hemarthrosis in hypocoagulable wild-type mice

A model of hemarthrosis with reversible hemostasis suppression in BALB/c mice (^{Hypo}BALB/c model) was used, as described previously [14], to elicit comparable joint bleeding to FVIII$^{-/-}$ mice. Briefly, BALB/cByJ mice were fed 7.5 to 10 μg/mL warfarin dissolved in drinking water for 7 days and injected intravenously with 0.25 mg/kg anti-FVIII (GMA-8015) to induce hypocoagulability 2 hours before knee injury. Hemarthrosis was induced by several subpatellar punctures of the right knee with a 30-gauge needle. On Day 2 after knee injury, warfarin was discontinued and mice were injected with 100 IU/kg 4-factor prothrombin complex concentrate (4F-PCC) [14] to reverse the effects of warfarin. The hematocrit was determined on Day 2 as a measure of joint bleeding and joint tissue was harvested at 2 and 4 weeks after injury.

2.4 Joint tissue harvest and Perls' Prussian blue staining

Joint tissue from injured FVIII$^{-/-}$ mice and ^{Hypo}BALB/c mice was fixed in 10% zinc-buffered formalin (Z-Fix) (Anatech, Battle Creek, MI) for 2 days with gentle shaking and decalcified in 10% (v/v) formic acid +/−0.2% (w/v) potassium ferrocyanide for Perls' Prussian blue staining of ferric iron (Fe^{3+}). Decalcified joints were processed, embedded in paraffin wax, and sectioned (4μm) for imaging and immunohistochemistry procedures [16]. After deparaffinization and mounting, Prussian blue-stained slides were imaged using a NanoZoomer 2.0-HT brightfield slide scanner at 20x magnification (Hamamatsu Photonics, Hamamatsu, Japan). Prussian blue staining was quantified in synovial tissue using ImageJ software (National Institutes of Health, Bethesda, MD, USA).

2.5 Immunohistochemistry/immunofluorescence

Immunohistochemistry was performed to detect CD68 as a marker for macrophages and macrophage-like synoviocytes (rabbit polyclonal anti-CD68 [ab125212]; abcam, Cambridge, MA, USA), α-smooth muscle actin (αSMA) as a marker for remodeling vessels (rabbit polyclonal anti-αSMA [ab5694]; abcam), and lymphatic vessel endothelial receptor 1 (LYVE1) as a marker for lymphatic vessels (goat polyclonal anti-LYVE1 [AF2125]; R&D Systems, Minneapolis, MN, USA) in synovial tissue. Primary antibodies were detected with ImmPress AP Horse Anti-Rabbit/Anti-Goat IgG Polymer Detection Kits and Vector Red Alkaline Phosphatase Substrate Kit (Vector Laboratories, Burlingame, CA, USA). Gross morphology and extravasated erythrocytes were visualized by Safranin-O-Fast Green staining [13, 14]. Slides were scanned using a NanoZoomer 2.0-HT brightfield slide scanner at 20x magnification. Tissue area and stained areas were quantified using ImageJ. For immunofluorescence, the same antibodies were used to detect LYVE1 and αSMA in synovium, followed by donkey anti-goat Alexa Fluor 647 and donkey anti-rabbit Alexa Fluor 594 (Jackson Immunoresearch, West Grove, PA, USA) secondary antibodies, respectively. Slides were mounted with media containing 4′,6-diamidino-2-phenylindole (DAPI) and imaged by laser scanning confocal microscopy on a Zeiss LSM 880 microscope (Zeiss, Oberkochen, Germany) at 10x magnification.

2.6 RNA sequencing

Synovial tissue was harvested from FVIII$^{-/-}$ mice at baseline, Day 3, and 2 weeks after injury. RNA isolation and RNA sequencing were performed as described previously and detailed briefly below [13, 14]. A NEBNext® Poly(A) mRNA Magnetic Isolation Module (New England Biolabs, Ipswich, MA, USA) was used for polyA selection of splenic RNA (100 ng), followed by library preparation with a NEBNext Ultra II Directional RNA Library Prep Kit (New England Biolabs). A SMART-Seq® v4 Ultra® Low Input RNA Kit (Takara Bio, Mountain View, CA, USA) was used to generate cDNA from total synovial RNA (8 ng) and libraries were generated using an NEBNext® Ultra™ II DNA Library Prep Kit (New England Biolabs). All cDNA libraries were cleaned using 0.9X AmPure XP Beads (New England Biolabs) and sequenced on a NextSeq500 system (Illumina, San Diego, CA, USA) (75bp; single-end) to generate approximately 20 million reads per sample. RNA sequencing was performed by the Institute for Genomic Medicine (IGM) Genomics Center at UCSD.

2.7 Sequencing data analysis

Primary RNAseq data analyses were carried out by UCSD Center for Computational Biology and Bioinformatics as described previously [13, 14]. FastQC v0.11.4 was used for quality control checks on raw sequencing data and Salmon v0.7.2 [25] was used for gene-level expression quantification. Subsequent analyses included trimmed mean of M-values (TMM) normalization [26], differential expression analyses using the limma-voom method [27], filtering lowly expressed genes (counts per million >1 in ≥10 samples), and controlling for batch effects. Significance was defined by an adjusted p-value <0.05 after multiple testing corrections using a moderated t-statistic in limma. Heat maps were generated using Morpheus (https://software.broadinstitute.org/morpheus).

2.8 Statistical analyses

Data are expressed as median plus interquartile range and statistical comparisons were made using the Kruskal-Wallis test with Dunn's multiple comparison test. Relationships between histological parameters were assessed using Spearman's rank correlation analysis. In all cases, a p-value <0.05 was considered statistically significant. For RNAseq data, the criteria for differential expression were i) $\log_2$ fold-change of magnitude >1 and ii) adjusted p-value <0.05.

3 Results

3.1 Hemarthrosis and synovial hypertrophy in FVIII$^{-/-}$ and ^{Hypo}BALB/c mice after knee injury

A schematic representation of the experimental groups is provided in Supplementary Figure 1. The use of the ^{Hypo}BALB/c model [14] in comparison to FVIII$^{-/-}$ mice provided the unique opportunity to study the effects of long-term intrinsic FVIII availability, after recovery from a temporary (few days) depletion of intrinsic FVIII activity (anti-FVIII antibody treatment), on iron clearance from the joint. The combined use of anti-FVIII antibody and warfarin (reversed 2 days post-bleed) to generate ^{Hypo}BALB/c mice was necessary, since warfarin or anti-FVIII antibody alone do not facilitate joint bleeding equal to FVIII$^{-/-}$ mice [28].

For injured FVIII$^{-/-}$ mice, the mean Day 2 hematocrit (joint bleeding) was similar for all saline-treated groups (~30%) and significantly lower compared to baseline (47.5%). Peri-procedural rhFVIII maintained hematocrits that were comparable to baseline. The mean Day 2 hematocrit for injured ^{Hypo}BALB/c mice (~34%) was comparable to injured FVIII$^{-/-}$ mice, as previously reported [14] (Supplementary Figure 2).

Synovial hypertrophy was determined histologically in harvested joint tissue by quantifying synovial tissue area (Supplementary Figure 3). Tissue area was expanded in all groups of injured FVIII$^{-/-}$ mice compared to baseline, peaking at 2 weeks after injury (2.5-fold increase, p=0.008). Despite the reduction in bleed volume, peri-procedural rhFVIII caused a similar expansion in tissue area at 2 weeks (2.6-fold, p=0.03) compared to saline-treated mice. Tissue expansion was mild in ^{Hypo}BALB/c mice at 2 and 4 weeks (1.2-fold and

1.6-fold, respectively; $p<0.05$) after knee injury compared to baseline, and lower than in FVIII$^{-/-}$ mice.

3.2 Iron accumulation in synovial tissue after knee injury in FVIII$^{-/-}$ and ^{Hypo}BALB/c mice

Using a sensitive method of Prussian blue staining during decalcification [16], ferric iron was quantified in synovial tissue at multiple time points from Day 3 to 6 weeks after knee injury. In FVIII$^{-/-}$ mice, there was a large increase in ferric iron accumulation at 2 weeks (331-fold, p=0.0003) and 4 weeks (466-fold, p=0.0009) after injury relative to baseline, with moderate levels persisting at 6 weeks (13-fold, p=0.01) (Figure 1A). Prussian blue levels at 2 weeks after injury in rhFVIII-treated mice were comparable to baseline levels (Figure 1 A), indicating that bleed prevention prevented iron accumulation. There was a positive correlation between synovial ferric iron levels and soft tissue area (r=0.4626, p=0.02) (Figure 1B), suggesting that iron accumulation and synovial hypertrophy are intertwined in FVIII$^{-/-}$ mice. The distribution of synovial ferric iron changed over time from a diffuse appearance at 2 weeks to distinct clusters of iron at later time points. Representative examples are depicted in Figure 1C. On Day 3 after injury, there was an abundance of erythrocytes in the joint space with visible hematomas but very little Prussian blue (Figure 1D), suggesting that iron from extravasated erythrocytes is converted to the ferric form between Day 3 and 2 weeks after injury.

In ^{Hypo}BALB/c mice, an increase in Prussian blue was observed at 2 weeks after injury (50-fold, p=0.01), which was significantly less (14-fold, p=0.03) than in FVIII$^{-/-}$ mice despite a similar bleed volume (Figure 1E). In contrast to FVIII$^{-/-}$ mice, the Prussian blue accumulation had subsided to near baseline levels at 4 weeks. This suggests that iron accumulation and clearance are not dependent on bleed volume and that these processes are impaired in FVIII$^{-/-}$ mice. Since FVIII deficiency was only transient in the ^{Hypo}BALB/c mice at the time of bleeding, but enduring in the FVIII$^{-/-}$ mice, iron clearance appears dependent on FVIII availability during the healing phase.

3.3 Differential gene expression of iron regulators in synovial tissue in FVIII$^{-/-}$ mice after knee injury

To investigate potential mechanisms of iron transport and clearance, we studied synovial gene expression changes after induced joint bleeding in FVIII$^{-/-}$ mice, +/−rhFVIII treatment, by RNAseq (n=3–5 per group). We previously published RNAseq results of differential gene expression pertaining to tissue and vascular remodeling [14]. Here, we explored gene expression changes relating to iron uptake and transport (Reactome pathway R-MMU-917937) [29] in synovium on Day 3 and 2 weeks after knee injury. Among 48 genes in the pathway, 13 were differentially expressed and their functions are listed in Table 1. Figure 2 provides a visual representation of expression changes for all genes in this pathway. The full list of genes with their respective $\log_2$ fold-change and adjusted p-values are provided in the supplementary information (Supplementary Table 1).

The expression levels were generally highest on Day 3 and fell to baseline at 2 weeks for approximately half of the genes. RhFVIII dampened the differential expression for most of

the genes but did not fully normalize the gene expression pattern despite negligible joint bleed volume (Supplementary Figure 2) and no ferric iron accumulation (Figure 1A).

The most highly upregulated gene was *Hmox1* (hemoxygenase-1), which exhibited a 31-fold increase in expression on Day 3 ($p=3.0\times10^{-6}$) and a 3-fold increase at 2 weeks (p=0.003), both compared to baseline. Upregulation on Day 3 was dampened with rhFVIII (8-fold, p<0.0001). Hemogygenase-1 is broadly expressed in various tissues, is induced by stressors such as reactive oxygen species [30], and also responsible for intracellular heme degradation, thereby reducing heme cytotoxicity [31]. A similar expression pattern was observed for *Atp6v0d2* (V-ATPase subunit D2 gene) (Table 1).

Conversely, there was a strong down-regulation of the gene encoding ceruloplasmin (*Cp*) (17-fold on Day 3, $p=5.4\times10^{-5}$), a ferroxidase working in tandem with ferroportin and hephaestin to facilitate iron export [32]. This effect was dampened by rhFVIII (8-fold down-regulation relative to baseline, $p=7.4\times10^{-5}$). The hephaestin (ceruloplasmin homolog) gene (*Heph*) was also down-regulated on Day 3 (5-fold, p=0.002) and 2 weeks (3-fold, p=0.01), and rhFVIII did not dampen this effect (Table 1). The iron exporter ferroportin (solute carrier family 40 member 1 [*Slc40a1*]) was not significantly affected. The profound downregulation of 2 of 3 major genes facilitating iron export (*Cp*, *Heph*), suggests a tendency towards intracellular iron retention in $FVIII^{-/-}$ mice post-bleed. Since the observed gene expression changes were only partially corrected by rhFVIII, they appeared to be triggered by small amounts of blood.

There was a 5-fold down-regulation of *Cd163* (encoding the macrophage hemoglobin scavenger) on Day 3 (p=0.03), persisting at 2 weeks (3-fold decrease, p=0.02) normalized by rhFVIII (no differential expression) at both time points (Table 1). *Cd163* is expressed on M2-polarized macrophages, exerting anti-inflammatory properties [33–35], which may have been hampered in saline-treated mice.

Other differentially expressed genes involved in iron recycling, but whose roles are less well described, included *Lcn2, Slc11a1*, Tfrc*, Aco1, Slc22a17,* and genes encoding V-ATPase. Their protein names and functions are displayed in Table 1.

3.4 Synovial macrophage infiltration and/or differentiation in relation to iron accumulation after joint injury in $FVIII^{-/-}$and ^{Hypo}BALB/c mice

Based on these findings we sought to examine the relationship between macrophage and iron accumulation in synovial tissue after joint bleeding. Infiltration of macrophages into inflamed hemophilic synovium has been described previously [12, 31]. Macrophages ingest iron by erythrophagocytosis and/or CD163 mediated scavenging of hemoglobin [36]. We studied a time course of CD68 expression in association with synovial ferric iron levels in $FVIII^{-/-}$ mice (+/−rhFVIII) and ^{Hypo}BALB/c mice.

In $FVIII^{-/-}$ mice, CD68 expression remained at baseline on Day 3 but was profoundly elevated at 2 weeks (40-fold, p<0.0001 and 4 weeks (14-fold, p=0>0.05) after injury, subsiding somewhat at 6 weeks (15-fold increase, p>0.05) (Figure 3A and B). As with Prussian blue staining, CD68-positive cells were dispersed throughout the synovium at 2

weeks but appeared clustered at 4 weeks and 6 weeks after injury (Figure 3A), largely co-localizing with ferric iron deposits (Figure 3D). This suggests synovial clustering of iron-laden macrophages between 2 and 4 weeks after injury. There was a strong positive correlation between synovial ferric iron and CD68 expression ($r=0.8992$, $p<0.0001$) (Figure 3E), further supporting a relationship between macrophage accumulation and ferric iron levels. RhFVIII prevented the increase in CD68 expression at 2 weeks (Figure 3B), which aligned with absent Prussian blue staining (Figure 1A). Ferric iron levels also correlated with the extent of synovial hypertrophy (Figure 1B), suggesting that synovial hypertrophy and accumulation of iron-laden pro-inflammatory macrophages are intertwined (Figure 1A, 3B, and 4A), resolving slowly. In ^{Hypo}BALB/c mice, CD68 expression increased at 2 weeks (5-fold, $p=0.02$), but was much lower than in FVIII$^{-/-}$ mice and returned to baseline at 4 weeks (Figure 3C) despite the similar bleed volumes. The mild increase in CD68 expression aligned with sparse iron deposits (Figure 1E) and absence of synovial swelling. Altogether the findings suggest exaggerated synovial hypertrophy and accumulation of iron-laden macrophages in FVIII$^{-/-}$ mice. Thus, clearance of iron-laden macrophages from inflamed synovium after a joint bleed may be dependent on FVIII availability during the healing phase.

3.5 Synovial blood vessel remodeling and density in relation to iron accumulation after joint injury in FVIII$^{-/-}$ and ^{Hypo}BALB/c mice

To investigate the effect of synovial iron accumulation on vascular remodeling and density, which has been associated with vascular permeability and re-bleeding in mice and humans with FVIII-deficiency [13, 14, 18, 37], αSMA expression was normalized to soft tissue area and expressed as the fold-increase over the median baseline value for FVIII$^{-/-}$ or BALB/c mice (Figure 4A). Raw data are displayed in Supplementary Figure 4A. The median baseline values for αSMA area were 789 pixel^2 (interquartile range [IQR]: 531–1534) and 1636 pixel^2 (IQR: 1487–1809) for FVIII$^{-/-}$ and ^{Hypo}BALB/c mice, respectively. The density of αSMA-positive (αSMA+) blood vessels increased 1.9-fold at 2 weeks after injury ($p<0.05$) in FVIII$^{-/-}$ mice and remained elevated during the 6-week observation period (2.2-fold increase) (Figure 4A), supporting previous evidence of prolonged vascular remodeling after hemophilic joint bleeding [13, 14, 18]. The density of αSMA+ vessels was weakly associated with ferric iron levels ($r=0.3615$, $p=0.08$) (Figure 4B), indicating that iron accumulation had no major effect on vascular remodeling. Mice treated with rhFVIII exhibited a similar fold-increase in αSMA+ vessel density (1.6-fold, $p<0.05$) to those receiving saline (Supplementary Figure 4). The fold-increase in αSMA+ vessel density in ^{Hypo}BALB/c mice at 2 weeks (1.6-fold, $p=0.02$) and 4 weeks (1.7-fold, $p=0.008$) was comparable to FVIII$^{-/-}$ mice (+/−rhFVIII) suggesting that even little bleeding can incite vascular remodeling.

3.6 Synovial lymphatic vessel remodeling and density in relation to iron accumulation after joint injury in FVIII$^{-/-}$ and ^{Hypo}BALB/c mice

Since synovial iron deposition in FVIII$^{-/-}$ mice was proportional to macrophage accumulation and synovial swelling, but had little effect on vascular remodeling, we sought to investigate its interplay with lymphatic vessel remodeling. Macrophages have been implicated in the dynamics of lymphangiogenesis, whereby the lymphatic system provides

a potential clearance mechanism for iron-laden macrophages and plays an important role in resolution of inflammation [38]. Lymphangiogenesis is affected in mice with inflammatory arthritis [39, 40], but has not yet been described in hemophilic mice. We therefore examined and quantified lymphatic endothelial cell marker, LYVE1, in FVIII$^{-/-}$ and ^{Hypo}BALB/c mice by immunohistochemistry.

Expression levels of LYVE1 were normalized to soft tissue area to calculate vessel density, expressed as the fold-increase over the median baseline value for FVIII$^{-/-}$ or BALB/c mice (Figure 4C). Raw data are displayed in Supplementary Figure 4B. In contrast to αSMA expression, there was a transient, dramatic reduction in LYVE1 expression after induced hemarthrosis in FVIII$^{-/-}$ mice (Figure 4C, Figure 5 and Supplementary Figure 4). LYVE1 expression was decreased 11.8-fold on Day 3 ($p=0.007$) and 1.7-fold at 2 weeks ($p>0.05$) relative to baseline (Figure 4C). A modest reduction in LYVE1 expression persisted up to 4 weeks, and returned to baseline thereafter. LYVE1 expression at 2 weeks in mice treated with rhFVIII was comparable to baseline (0.9-fold increase, $p>0.05$). There was a strong negative correlation between lymphatic vessel density and Prussian blue staining ($r=0.6863$, $p<0.0001$) (Figure 4D). Representative examples of LYVE1 expression in relation to Prussian blue staining over the 6-week time course are displayed in Figure 5A. At baseline, LYVE1 expression revealed vessels appearing as small, incongruent structures (Figure 5A and B). In injured synovium, lymphatic vessels evolved into longer, flat structures that were distinct from αSMA+ vessels (Figure 5C).

^{Hypo}BALB/c mice had a higher median baseline LYVE1 area (12598 pixel^2; IQR: 11448–14695) compared to FVIII$^{-/-}$ mice (7028 pixel^2; IQR: 5296–8487) and, in contrast to FVIII$^{-/-}$ mice, maintained their baseline LYVE1 expression at 2 weeks and 4 weeks after injury. They also exhibited a 2.3-fold higher fold-increase in LYVE1 expression at 2 weeks than FVIII$^{-/-}$ mice ($p=0.009$) (Figure 4C).

These findings suggest a deficit in lymphangiogenesis in FVIII$^{-/-}$ mice, with a profoundly maladaptive response to injury-related hemarthrosis. Synovial iron accumulation was proportional to impairment of lymphangiogenesis, suggesting that lymphatic vessels contribute to tissue iron clearance.

3.7 Differential gene expression of lymphatic markers in synovial tissue after joint injury in FVIII$^{-/-}$ mice

To explore effects of joint bleeding on lymphangiogenesis in FVIII$^{-/-}$ mice, we pursued gene expression analyses by RNA sequencing. Several lymphatic markers showed pronounced transcriptomic changes after joint bleeding (Figure 6), demonstrating the incitement of processes related to lymphatic vessel remodeling at the molecular level. These genes are listed with their functions in Table 2, and the $\log_2$ fold-change and adjusted p-values for each gene are provided in the supplementary information (Supplementary Table 2). RhFVIII dampened the differential expression for most genes but did not fully normalize the gene expression pattern despite negligible joint bleed volume (Supplementary Figure 2).

The chemokine (C-C motif) ligand 21 gene (*Ccl21*) was 194-fold upregulated at 2 weeks ($p=0.001$), coinciding with the increased CD68 expression in synovium at 2 weeks (Figure

3A/B). The CCL21 protein is expressed by synovial fibroblasts in inflammatory arthritis [41] and functions as a chemoattractant for chemokine receptor 7 expressing cells, such as macrophages. It is also constitutively expressed on lymphatic endothelial cells (LECs) [42]. *Ccl21* upregulation may therefore play a central role in macrophage infiltration in inflamed synovium, as well as macrophage trafficking to lymphatic vessels. The *Sema7a* gene (encoding semaphorin 7a), was 20-fold (p=0.0003) and 5-fold (p=0.02) upregulated on Day 3 and 2 weeks, respectively, promoting chemokine-driven immune cell and macrophage migration [43]. Other upregulated genes included *Ccbe1* (collagen and calcium binding EGF domains 1), which functions in lymphatic vessel maturation; *Flt4*, which encodes a receptor for vascular endothelial growth factor (VEGF)C and VEGFD; and *Nrp2,* which also encodes a receptor (neuropilin-2) for VEGFC and mediates VEGFC-induced lymphatic sprouting. However, the *Vegfc* and *Vegfd* genes were downregulated (≈2 to 5-fold). Moreover, *Lyve1* was 37-fold and 7-fold (both p=0.0001) down-regulated on Day 3 and 2 weeks, respectively. These findings align with the reduction in LYVE1 expression and lymphatic vessel density observed histologically (Figure 4C, Figure 5, and Supplementary Figure 4).

Of note, rhFVIII dampened the downregulation of *Lyve1* on Day 3 (from 37-fold to 6-fold), normalized *Nrp2*, *Sema7a* and *Vegfd* expression at 2 weeks, and increased *Vegfc* expression (from 2-fold downregulated to 2-fold upregulated) on Day 3 and at 2 weeks. These findings imply that rhFVIII restored the neuropilin-2/VEGFC axis (critical for lymphatic vessel sprouting), and improved *Lyve1* gene expression sufficient to normalize LYVE1 protein expression (Figure 5C).

4 Discussion

It is generally accepted that iron accumulation in association with hemophilic joint bleeding is the incendiary propelling HA progression. Iron accumulation in HA demonstrated by magnetic resonance imaging or Prussian blue staining is assumed to be the result of frequent joint bleeding over time [44]. However, it has never been questioned if impairment of iron clearance may contribute to hemosiderin accumulation, perhaps due to joint inflammation affecting synovial iron handling and/or other unknown features related to hemophilia.

Here, we shed light on this question by studying synovial iron accumulation and clearance rates in FVIII$^{-/-}$ mice. We employed two established mouse models involving induced knee bleeding in FVIII$^{-/-}$ (BALB/c background) and ^{Hypo}BALB/c mice [14], and compared iron accumulation and clearance rates. FVIII$^{-/-}$ and ^{Hypo}BALB/c mice share the peri-procedural lack of intrinsic FVIII activity with comparable joint bleed volumes after knee injury. FVIII deficiency is transient in ^{Hypo}BALB/c mice owing to rapid clearance of anti-FVIII antibody, but permanent in FVIII$^{-/-}$ mice, thereby enabling the investigation of the long-term effects of FVIII on synovial iron clearance.

We discovered that, compared to transient FVIII deficiency (^{Hypo}BALB/c mice), permanent FVIII deficiency (FVIII$^{-/-}$ mice) was associated with a profound inability to clear synovial iron during the 6-week observation period, accompanied by prominent synovial hypertrophy, macrophage accumulation, and impairment of lymphangiogenesis. These findings could be largely abrogated by bleed prevention with peri-procedural rhFVIII treatment, excluding

that needle injury alone, perhaps followed by subclinical blood leakage, may have resulted in iron accumulation. Of note though, peri-procedural rhFVIII treatment did not reduce synovial tissue swelling and, as also shown earlier [14], synovial vascularity, suggesting that small blood volumes or injury may be sufficient to trigger synovitis, which is not avoidable by short-term factor replacement.

Macrophages belong to the reticuloendothelial system and facilitate iron recycling. Macrophages engulf and digest erythrocytes, scavenge hemoglobin via the CD163 receptor, degrade heme, and oxidize toxic Fe^{2+} to less toxic Fe^{3+} via inducible hemoxygenase [45, 46]. Here, we demonstrated that the extent of macrophage (CD68 expression) and ferric iron (Prussian blue) accumulation correlated well in FVIII$^{-/-}$ mice, with co-localization over time, suggesting reticuloendothelial macrophage recruitment and iron uptake in response to hemarthrosis. However, the magnitude of synovial iron and macrophage accumulation in FVIII$^{-/-}$ mice vastly exceeded that of ^{Hypo}BALB/c mice. Moreover, iron clearance was incomplete during the 6-week observation period, while iron became quickly undetectable in ^{Hypo}BALB/c mice.

Tissue drainage of debris, interstitial fluid, macromolecules, and immune cells including macrophages is accomplished through the lymphatic system [47–50]. The lymphatics serve as a conduit for macrophage and immune cell movement to local and distant lymph nodes [47]. Alteration of lymphangiogenesis has been noted in rheumatoid arthritis (RA) and osteoarthritis, and thought to be an under-recognized mechanism contributing to disease manifestations. Although the molecular regulation of the synovial lymphatic system is incompletely understood, it has been established that functional lymphatics are critical for tissue homeostasis [47, 51]. The formation of lymph vessels requires VEGFC, provided by activated macrophages attracted by LECs [47, 51]. Lymphatics are affected negatively in murine RA, and their restoration by anti-TNF therapy was critical to facilitate removal of macrophages and other inflammatory cells [52]. Although little is known about excess tissue iron removal after hematoma formation, two clinical reports describe that iron-laden macrophages use lymphatics to exit tissue [53, 54]. Altogether, this prompted us to probe if lymphatic dysregulation may play a role in the impaired removal of iron from synovial tissue in FVIII$^{-/-}$ mice. Indeed, FVIII$^{-/-}$ mice exhibited lower synovial LYVE1 expression at baseline compared to ^{Hypo}BALB/c mice, with a significant decrease shortly after hemarthrosis and incomplete recovery even 4 weeks later. LEC rarefication was associated with pronounced iron and macrophage accumulation, both of which diminished with increasing LYVE1 expression over time and with formation of tubular lymphatic structures. As these findings were not present in ^{Hypo}BALB/c mice despite similar joint bleed volumes, it appears that lymphangiogenic dysregulation in FVIII$^{-/-}$ mice contributed to impaired synovial iron clearance. The temporal relationship of lymphatic capillary formation and disappearance of iron-laden macrophages also suggest that the lymphatics (and not blood vessels) constitute an important pathway for removal of iron-laden macrophages from synovium. This is further supported by the fact that the extent of vascularity (αSMA-expressing blood vessels) was comparable between FVIII$^{-/-}$ and ^{Hypo}BALB/c mice and did not correlate with iron accumulation. These findings imply that FVIII deficiency disrupted lymphangiogenesis and synovial iron clearance during the healing phase; however, the reasons for this lymphaniogenic dysregulation are less clear.

Differential gene expression analyses were helpful to formulate hypotheses connecting molecular processes related to synovial iron recycling and lymphangiogenesis. First, the analyses established that gene expression patterns involving molecular processes of iron handling and transport were highly affected in hemophilic synovium after hemarthrosis, although analyses were not cell-type specific. Second, gene expression changes related to lymphangiogenesis strengthened histological findings. The genes encoding *Lyve1* and *Vegfc/d* were downregulated after hemarthrosis. Upregulation of *Flt4* and *Nrp2* genes encoding the VEGFC/D receptors could not compensate to instigate histologically detectable lymphatic sprouting. Of note, avoidance of large hematoma formation with peri-procedural rhFVIII mitigated *Lyve1* downregulation, maintained baseline levels of LYVE1 protein expression, and reversed *Vegfc* gene expression from down-regulated to upregulated (Table 2). These findings support a central role of VEGFC in synovial lymphangiogenesis [47], but do not explain why VEGFC-modulated lymphangiogenesis is disrupted after hemarthrosis in FVIII$^{-/-}$ mice. One explanation may be inherent to recent reports that FVIII gene and protein expression is high in LECs compared to other endothelial cell populations [55, 56]. However, FVIII activity in the lymph is only ≈10–30% of that in plasma, perhaps due to low secretion with low lymphatic shear stress [56]. It is conceivable that FVIII expression in LECs is important for lymphangiogenesis and/or adaptive lymphatic processes. Mechanical signals, including fluidity within vessels, are deemed important regulators of lymphangiogenesis and lymphatic vessel integrity [57]. Although lymph is hypocoagulable due to the absence of platelets and reduced clotting factor activities and fibrinogen [58], one may speculate that undercutting thresholds of lymph coagulability by absence of FVIII may affect flow dynamics and adaptive lymphangiogenesis.

When analyzing synovial gene expression of iron regulators in FVIII$^{-/-}$ mice, significant differential expression of genes involved in heme scavenging, heme degradation, and iron export ensued after hemarthrosis. Many of those genes exert dual roles in inflammation. Here, their expression pattern inferred a pro-inflammatory milieu (for instance upregulation of *Hmox1*, downregulation of *Cd163*). Also, iron export gene regulation appeared tilted towards intracellular iron containment, a characteristic innate host response to deprive intruding organisms of iron [46]. Since inflammation may curtail lymphatic vessel formation and drainage [59], shown previously to influence VEGFC/D secretion by macrophages and their biological functions [60–62], the here observed downregulation of *vegfc/d* in FVIII$^{-/-}$ mice (reversible with rhFVIII/bleed rescue) suggests that the post-bleed inflammatory milieu contributed at least in part to lymphangiogenesis dysregulation.

5 Conclusions

Our observations suggest maladaptive lymphangiogenesis in response to hemarthrosis in FVIII deficiency, resulting in synovial iron accumulation by curtailing lymph-mediated exit of iron-laden macrophages. Dysregulated lymphangiogenesis has been shown to increase joint inflammation and lesions profoundly in other arthritic conditions [40], with notable improvement upon restoration of lymphatic drainage [63]. Therefore, studying and targeting lymphatic function as a novel target in HA, and investigating whether defective lymphangiogenesis is unique to FVIII deficiency or is also present in Factor IX deficiency, appear important next steps.

Supplementary Material

Refer to Web version on PubMed Central for supplementary material.

Acknowledgements

This study was funded by a Career Development Award from the National Hemophilia Foundation (NHF) (AvD), the NHF/Nicholas Cirelli Family Research Fund Judith Graham Pool Research Fellowship (EJC), Bioverativ/Sanofi (AvD), and National Institutes of Health grant UL1TR001442 of CTSA (KMF). Slide scanning and confocal microscopy were performed at the School of Medicine Microscopy Core, University of California San Diego, which is supported by grant NS047101. We thank Eric Y Chang for providing histology equipment, and Jonathan H Wong for his assistance with histology work and experimental design for ferric iron detection.

References

[1]. Cafuir L, Kruse-Jarres R, Mancuso ME, Kempton CL. Emicizumab for hemophilia A without inhibitors. Expert Review of Hematology. 2019; 12: 515–24. 10.1080/17474086.2019.1624519. [PubMed: 31130012]

[2]. Di Minno MND, Minno AD, Calcaterra I, Cimino E, Dell'Aquila F, Franchini M. Enhanced Half-Life Recombinant Factor VIII Concentrates for Hemophilia A: Final Results from Extension Studies. Semin Thromb Hemost. 2022; 48: 253–5. 10.1055/s-0041-1740148. [PubMed: 34942666]

[3]. Gualtierotti R, Solimeno LP, Peyvandi F. Hemophilic arthropathy: Current knowledge and future perspectives. J Thromb Haemost. 2021; 19: 2112–21. 10.1111/jth.15444. [PubMed: 34197690]

[4]. Wyseure T, Mosnier LO, von Drygalski A. Advances and challenges in hemophilic arthropathy. Semin Hematol. 2016; 53: 10–9. 10.1053/j.seminhematol.2015.10.005. [PubMed: 26805902]

[5]. Gammella E, Recalcati S, Cairo G. Dual Role of ROS as Signal and Stress Agents: Iron Tips the Balance in favor of Toxic Effects. Oxid Med Cell Longev. 2016; 2016: 8629024. 10.1155/2016/8629024. [PubMed: 27006749]

[6]. Fabry G. Ultrastructural changes in synovium and cartilage in experimental hemarthrosis in dogs. Arch Orthop Trauma Surg. 1990; 109: 21–9. 10.1007/bf00441905. [PubMed: 2344263]

[7]. Roosendaal G, Vianen ME, Wenting MJ, van Rinsum AC, van den Berg HM, Lafeber FP, Bijlsma JW. Iron deposits and catabolic properties of synovial tissue from patients with haemophilia. J Bone Joint Surg Br. 1998; 80: 540–5. 10.1302/0301-620x.80b3.7807. [PubMed: 9619953]

[8]. van Vulpen LF, Roosendaal G, van Asbeck BS, Mastbergen SC, Lafeber FP, Schutgens RE. The detrimental effects of iron on the joint: a comparison between haemochromatosis and haemophilia. J Clin Pathol. 2015; 68: 592–600. 10.1136/jclinpath-2015-202967. [PubMed: 25897098]

[9]. Wen FQ, Jabbar AA, Chen YX, Kazarian T, Patel DA, Valentino LA. c-myc proto-oncogene expression in hemophilic synovitis: in vitro studies of the effects of iron and ceramide. Blood. 2002; 100: 912–6. 10.1182/blood-2002-02-0390. [PubMed: 12130502]

[10]. Hakobyan N, Kazarian T, Jabbar AA, Jabbar KJ, Valentino LA. Pathobiology of hemophilic synovitis I: overexpression of mdm2 oncogene. Blood. 2004; 104: 2060–4. 10.1182/blood-2003-12-4231. [PubMed: 15172967]

[11]. Sen D, Chapla A, Walter N, Daniel V, Srivastava A, Jayandharan GR. Nuclear factor (NF)-κB and its associated pathways are major molecular regulators of blood-induced joint damage in a murine model of hemophilia. Journal of Thrombosis and Haemostasis. 2013; 11: 293–306. 10.1111/jth.12101. [PubMed: 23231432]

[12]. Narkbunnam N, Sun J, Hu G, Lin FC, Bateman TA, Mihara M, Monahan PE. IL-6 receptor antagonist as adjunctive therapy with clotting factor replacement to protect against bleeding-induced arthropathy in hemophilia. J Thromb Haemost. 2013; 11: 881–93. 10.1111/jth.12176. [PubMed: 23413986]

[13]. Cooke EJ, Zhou JY, Wyseure T, Joshi S, Bhat V, Durden DL, Mosnier LO, von Drygalski A. Vascular Permeability and Remodelling Coincide with Inflammatory and Reparative Processes

after Joint Bleeding in Factor VIII-Deficient Mice. Thromb Haemost. 2018; 118: 1036–47. 10.1055/s-0038-1641755. [PubMed: 29847841]

[14]. Cooke EJ, Wyseure T, Zhou JY, Gopal S, Nasamran CA, Fisch KM, Manon-Jensen T, Karsdal MA, Mosnier LO, von Drygalski A. Mechanisms of vascular permeability and remodeling associated with hemarthrosis in factor VIII-deficient mice. J Thromb Haemost. 2019; 17: 1815–26. 10.1111/jth.14567. [PubMed: 31301687]

[15]. Pulles AE, Mastbergen SC, Schutgens RE, Lafeber FP, van Vulpen LF. Pathophysiology of hemophilic arthropathy and potential targets for therapy. Pharmacol Res. 2017; 115: 192–9. 10.1016/j.phrs.2016.11.032. [PubMed: 27890816]

[16]. Zhou JY, Wong JH, Berman ZT, Lombardi AF, Chang EY, von Drygalski A. Bleeding with iron deposition and vascular remodelling in subchondral cysts: A newly discovered feature unique to haemophilic arthropathy. Haemophilia. 2021; 27: e730–e8. 10.1111/hae.14417. [PubMed: 34537999]

[17]. von Drygalski A, Barnes RFW, Jang H, Ma Y, Wong JH, Berman Z, Du J, Chang EY. Advanced magnetic resonance imaging of cartilage components in haemophilic joints reveals that cartilage hemosiderin correlates with joint deterioration. Haemophilia. 2019; 25: 851–8. 10.1111/hae.13802. [PubMed: 31199035]

[18]. Bhat V, Olmer M, Joshi S, Durden DL, Cramer TJ, Barnes RF, Ball ST, Hughes TH, Silva M, Luck JV, Moore RE, Mosnier LO, von Drygalski A. Vascular remodeling underlies rebleeding in hemophilic arthropathy. Am J Hematol. 2015; 90: 1027–35. 10.1002/ajh.24133. [PubMed: 26257191]

[19]. Nieuwenhuizen L, Schutgens RE, van Asbeck BS, Wenting MJ, van Veghel K, Roosendaal G, Biesma DH, Lafeber FP. Identification and expression of iron regulators in human synovium: evidence for upregulation in haemophilic arthropathy compared to rheumatoid arthritis, osteoarthritis, and healthy controls. Haemophilia. 2013; 19: e218–27. 10.1111/hae.12208. [PubMed: 23777533]

[20]. Weiss G, Ganz T, Goodnough LT. Anemia of inflammation. Blood. 2019; 133: 40–50. 10.1182/blood-2018-06-856500. [PubMed: 30401705]

[21]. Pulles AE, van Vulpen LFD, Coeleveld K, Mastbergen SC, Schutgens REG, Lafeber F. On-demand treatment with the iron chelator deferasirox is ineffective in preventing blood-induced joint damage in haemophilic mice. Haemophilia. 2021; 27: 648–56. 10.1111/hae.14328. [PubMed: 34043875]

[22]. Nieuwenhuizen L, Roosendaal G, Mastbergen SC, Coeleveld K, Biesma DH, Lafeber FP, Schutgens RE. Deferasirox limits cartilage damage following haemarthrosis in haemophilic mice. Thromb Haemost. 2014; 112: 1044–50. 10.1160/th14-01-0029. [PubMed: 25182505]

[23]. Brown BD, Shi CX, Rawle FE, Tinlin S, McKinven A, Hough C, Graham FL, Lillicrap D. Factors influencing therapeutic efficacy and the host immune response to helper-dependent adenoviral gene therapy in hemophilia A mice. Journal of thrombosis and haemostasis : JTH. 2004; 2: 111–8. [PubMed: 14717974]

[24]. von Drygalski A, Cramer TJ, Bhat V, Griffin JH, Gale AJ, Mosnier LO. Improved hemostasis in hemophilia mice by means of an engineered factor Va mutant. Journal of thrombosis and haemostasis : JTH. 2014; 12: 363–72. 10.1111/jth.12489. [PubMed: 24818532]

[25]. Patro R, Duggal G, Love MI, Irizarry RA, Kingsford C. Salmon provides fast and bias-aware quantification of transcript expression. Nature methods. 2017; 14: 417–9. 10.1038/nmeth.4197. [PubMed: 28263959]

[26]. Robinson MD, Oshlack A. A scaling normalization method for differential expression analysis of RNA-seq data. Genome Biol. 2010; 11: R25. 10.1186/gb-2010-11-3-r25. [PubMed: 20196867]

[27]. Law CW, Chen Y, Shi W, Smyth GK. voom: Precision weights unlock linear model analysis tools for RNA-seq read counts. Genome biology. 2014; 15: R29. 10.1186/gb-2014-15-2-r29. [PubMed: 24485249]

[28]. Wyseure T, Cooke EJ, Declerck PJ, Behrendt N, Meijers JCM, von Drygalski A, Mosnier LO. Defective TAFI activation in hemophilia A mice is a major contributor to joint bleeding. Blood. 2018; 132: 1593–603. 10.1182/blood-2018-01-828434. [PubMed: 30026184]

[29]. Jassal B, Matthews L, Viteri G, Gong C, Lorente P, Fabregat A, Sidiropoulos K, Cook J, Gillespie M, Haw R, Loney F, May B, Milacic M, Rothfels K, Sevilla C, Shamovsky V, Shorser S, Varusai T, Weiser J, Wu G, Stein L, Hermjakob H, D'Eustachio P. The reactome pathway knowledgebase. Nucleic acids research. 2020; 48: D498–D503. 10.1093/nar/gkz1031. [PubMed: 31691815]

[30]. Silva R, Vasconcelos LR, Travassos LH. The different facets of heme-oxygenase 1 in innate and adaptive immunity. Cell Biochem Biophys. 2022; 80: 609–31. 10.1007/s12013-022-01087-z. [PubMed: 36018440]

[31]. Acharya SS, Kaplan RN, Macdonald D, Fabiyi OT, DiMichele D, Lyden D. Neoangiogenesis contributes to the development of hemophilic synovitis. Blood. 2011; 117: 2484–93. 10.1182/blood-2010-05-284653. [PubMed: 21163925]

[32]. Yang Q, Liu W, Zhang S, Liu S. The cardinal roles of ferroportin and its partners in controlling cellular iron in and out. Life Sci. 2020; 258: 118135. 10.1016/j.lfs.2020.118135. [PubMed: 32712297]

[33]. Austermann J, Roth J, Barczyk-Kahlert K. The Good and the Bad: Monocytes' and Macrophages' Diverse Functions in Inflammation. Cells. 2022; 11. 10.3390/cells11121979.

[34]. Cutolo M, Campitiello R, Gotelli E, Soldano S. The Role of M1/M2 Macrophage Polarization in Rheumatoid Arthritis Synovitis. Front Immunol. 2022; 13: 867260. 10.3389/fimmu.2022.867260. [PubMed: 35663975]

[35]. Svendsen P, Etzerodt A, Deleuran BW, Moestrup SK. Mouse CD163 deficiency strongly enhances experimental collagen-induced arthritis. Scientific Reports. 2020; 10: 12447. 10.1038/s41598-020-69018-7. [PubMed: 32710083]

[36]. Sukhbaatar N, Weichhart T. Iron Regulation: Macrophages in Control. Pharmaceuticals (Basel). 2018; 11. 10.3390/ph11040137.

[37]. Kidder W, Chang EY, C MM, Rose SC, von Drygalski A. Persistent Vascular Remodeling and Leakiness are Important Components of the Pathobiology of Re-bleeding in Hemophilic Joints: Two Informative Cases. Microcirculation. 2016; 23: 373–8. 10.1111/micc.12273. [PubMed: 26833634]

[38]. Stritt S, Koltowska K, Mäkinen T. Homeostatic maintenance of the lymphatic vasculature. Trends Mol Med. 2021; 27: 955–70. 10.1016/j.molmed.2021.07.003. [PubMed: 34332911]

[39]. Zhang Q, Lu Y, Proulx ST, Guo R, Yao Z, Schwarz EM, Boyce BF, Xing L. Increased lymphangiogenesis in joints of mice with inflammatory arthritis. Arthritis research & therapy. 2007; 9: R118. 10.1186/ar2326. [PubMed: 17997858]

[40]. Guo R, Zhou Q, Proulx ST, Wood R, Ji RC, Ritchlin CT, Pytowski B, Zhu Z, Wang YJ, Schwarz EM, Xing L. Inhibition of lymphangiogenesis and lymphatic drainage via vascular endothelial growth factor receptor 3 blockade increases the severity of inflammation in a mouse model of chronic inflammatory arthritis. Arthritis Rheum. 2009; 60: 2666–76. 10.1002/art.24764. [PubMed: 19714652]

[41]. Pickens SR, Chamberlain ND, Volin MV, Pope RM, Mandelin AM 2nd, Shahrara S. Characterization of CCL19 and CCL21 in rheumatoid arthritis. Arthritis Rheum. 2011; 63: 914–22. 10.1002/art.30232. [PubMed: 21225692]

[42]. Farnsworth RH, Karnezis T, Maciburko SJ, Mueller SN, Stacker SA. The Interplay Between Lymphatic Vessels and Chemokines. Frontiers in immunology. 2019; 10: 518. 10.3389/fimmu.2019.00518. [PubMed: 31105685]

[43]. van Rijn A, Paulis L, te Riet J, Vasaturo A, Reinieren-Beeren I, van der Schaaf A, Kuipers AJ, Schulte LP, Jongbloets BC, Pasterkamp RJ, Figdor CG, van Spriel AB, Buschow SI. Semaphorin 7A Promotes Chemokine-Driven Dendritic Cell Migration. Journal of immunology. 2016; 196: 459–68. 10.4049/jimmunol.1403096.

[44]. Lundin B, Manco-Johnson ML, Ignas DM, Moineddin R, Blanchette VS, Dunn AL, Gibikote SV, Keshava SN, Ljung R, Manco-Johnson MJ, Miller SF, Rivard GE, Doria AS, Group TIPS. An MRI scale for assessment of haemophilic arthropathy from the International Prophylaxis Study Group. Haemophilia. 2012; 18: 962–70. 10.1111/j.1365-2516.2012.02883.x. [PubMed: 22765835]

[45]. Recalcati S, Cairo G. Macrophages and Iron: A Special Relationship. Biomedicines. 2021; 9. 10.3390/biomedicines9111585.

[46]. Mertens C, Marques O, Horvat NK, Simonetti M, Muckenthaler MU, Jung M. The Macrophage Iron Signature in Health and Disease. Int J Mol Sci. 2021; 22. 10.3390/ijms22168457.

[47]. Bouta EM, Bell RD, Rahimi H, Xing L, Wood RW, Bingham CO 3rd, Ritchlin CT, Schwarz EM. Targeting lymphatic function as a novel therapeutic intervention for rheumatoid arthritis. Nat Rev Rheumatol. 2018; 14: 94–106. 10.1038/nrrheum.2017.205. [PubMed: 29323343]

[48]. Magold AI, Swartz MA. Pathogenic Exploitation of Lymphatic Vessels. Cells. 2022; 11. 10.3390/cells11060979.

[49]. Olszewski WL. The lymphatic system in body homeostasis: physiological conditions. Lymphat Res Biol. 2003; 1: 11–21; discussion −4. 10.1089/15396850360495655. [PubMed: 15624317]

[50]. Randolph GJ, Angeli V, Swartz MA. Dendritic-cell trafficking to lymph nodes through lymphatic vessels. Nat Rev Immunol. 2005; 5: 617–28. 10.1038/nri1670. [PubMed: 16056255]

[51]. Cao M, Ong MTY, Yung PSH, Tuan RS, Jiang Y. Role of synovial lymphatic function in osteoarthritis. Osteoarthritis Cartilage. 2022; 30: 1186–97. 10.1016/j.joca.2022.04.003. [PubMed: 35487439]

[52]. Bouta EM, Kuzin I, de Mesy Bentley K, Wood RW, Rahimi H, Ji RC, Ritchlin CT, Bottaro A, Xing L, Schwarz EM. Brief Report: Treatment of Tumor Necrosis Factor-Transgenic Mice With Anti-Tumor Necrosis Factor Restores Lymphatic Contractions, Repairs Lymphatic Vessels, and May Increase Monocyte/Macrophage Egress. Arthritis Rheumatol. 2017; 69: 1187–93. 10.1002/art.40047. [PubMed: 28118521]

[53]. Caversaccio M, Peschel O, Arnold W. The drainage of cerebrospinal fluid into the lymphatic system of the neck in humans. ORL J Otorhinolaryngol Relat Spec. 1996; 58: 164–6. 10.1159/000276818. [PubMed: 8797221]

[54]. Oehmichen M, Schmidt V. [Erythrocytes in cervical lymph nodes of the human as a sequela of stasis and/or lymph drainage. Questionable diagnostic significance in strangulation and mechanical injuries of the head]. Z Rechtsmed. 1989; 103: 33–41. 10.1007/bf01255844. [PubMed: 2588817]

[55]. Pan J, Dinh TT, Rajaraman A, Lee M, Scholz A, Czupalla CJ, Kiefel H, Zhu L, Xia L, Morser J, Jiang H, Santambrogio L, Butcher EC. Patterns of expression of factor VIII and von Willebrand factor by endothelial cell subsets in vivo. Blood. 2016; 128: 104–9. 10.1182/blood-2015-12-684688. [PubMed: 27207787]

[56]. Hough C, Notley C, Mo A, Videl B, Lillicrap D. Heterogeneity and reciprocity of FVIII and VWF expression, and the response to shear stress in cultured human endothelial cells. J Thromb Haemost. 2022; 20: 2507–18. 10.1111/jth.15841. [PubMed: 35950488]

[57]. Ujiie N, Kume T. Mechanical forces in lymphatic vessel development: Focus on transcriptional regulation. Front Physiol. 2022; 13: 1066460. 10.3389/fphys.2022.1066460. [PubMed: 36439271]

[58]. Lippi G, Favaloro EJ, Cervellin G. Hemostatic properties of the lymph: relationships with occlusion and thrombosis. Semin Thromb Hemost. 2012; 38: 213–21. 10.1055/s-0032-1301418. [PubMed: 22422335]

[59]. Card CM, Yu SS, Swartz MA. Emerging roles of lymphatic endothelium in regulating adaptive immunity. J Clin Invest. 2014; 124: 943–52. 10.1172/jci73316. [PubMed: 24590280]

[60]. Kerjaschki D. The crucial role of macrophages in lymphangiogenesis. J Clin Invest. 2005; 115: 2316–9. 10.1172/jci26354. [PubMed: 16138185]

[61]. Maruyama K, Ii M, Cursiefen C, Jackson DG, Keino H, Tomita M, Van Rooijen N, Takenaka H, D'Amore PA, Stein-Streilein J, Losordo DW, Streilein JW. Inflammation-induced lymphangiogenesis in the cornea arises from CD11b-positive macrophages. J Clin Invest. 2005; 115: 2363–72. 10.1172/jci23874. [PubMed: 16138190]

[62]. Ji RC. Macrophages are important mediators of either tumor- or inflammation-induced lymphangiogenesis. Cell Mol Life Sci. 2012; 69: 897–914. 10.1007/s00018-011-0848-6. [PubMed: 21984600]

[63]. Zhou Q, Guo R, Wood R, Boyce BF, Liang Q, Wang YJ, Schwarz EM, Xing L. Vascular endothelial growth factor C attenuates joint damage in chronic inflammatory arthritis by accelerating local lymphatic drainage in mice. Arthritis Rheum. 2011; 63: 2318–28. 10.1002/art.30421. [PubMed: 21538325]

Essentials

1. Frequent hemarthroses result in iron accumulation in hemophilic joints. However, mechanisms and time course of synovial iron clearance are unknown.
2. Induced hemarthrosis in FVIII$^{-/-}$ mice and hypocoagulable mice (warfarin and transient anti-FVIII antibody) to compare synovial iron clearance in relation to lymphangiogenesis. Molecular mechanisms were explored by RNAseq.
3. Profound defects in adaptive lymphangiogenesis after hemarthrosis, preventing iron clearance, were unique to hemophilic mice.
4. Intact lymphangiogenesis is critical for clearance of iron-laden macrophages, and these processes are dependent on FVIII availability during the healing phase.

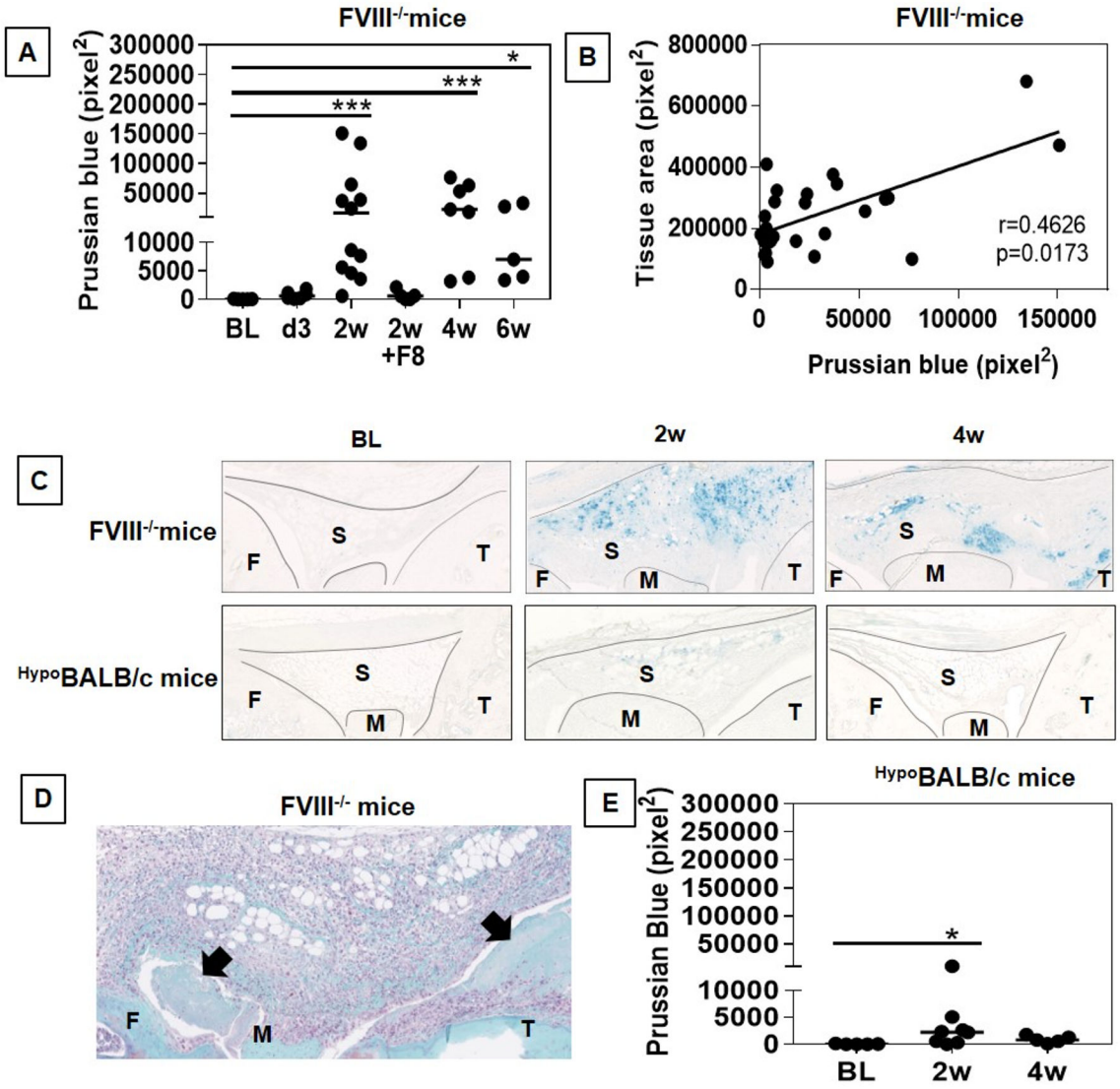

Figure 1. Ferric iron accumulation in synovial tissue after induced hemarthrosis.

Joint tissue was harvested from FVIII$^{-/-}$ and ^{Hypo}BALB/c mice at baseline (BL) and Day 3 (d3), 2 weeks (2w), 4 weeks (4w), or 6 weeks (6w) after sub-patellar injury to induce hemarthrosis (n=5–12 per group). A group of FVIII$^{-/-}$ mice received peri-procedural recombinant human FVIII before injury with tissue harvest at 2 weeks (2w+F8). Joint tissue was processed and stained with Perls Prussian blue for detection of ferric iron (Fe^{3+}). Paraffin-embedded tissue was sectioned (4μm), deparaffinized, and imaged using a Hamamatsu Nanozoomer brightfield slide scanner at 20x magnification. Prussian blue staining was quantified in synovial tissue using ImageJ. (A) Synovial iron quantification in FVIII$^{-/-}$ mice; (B) Spearman's rank correlation analysis between Prussian blue staining at 2 to 6 weeks after injury and soft tissue area in FVIII-deficient mice (n=30); (C) representative examples of synovial ferric iron staining; (D) representative Safranin O-Fast Green-stained joint tissue showing erythrocyte-laden synovium (green cells) with hematomas (black arrows) on Day 3 after injury; (E) synovial iron quantification in HypoBALB/c mice. Data

are displayed as median (*p<0.05, ***p<0.001). F: femur, S: synovium, M: meniscus, T: tibia.

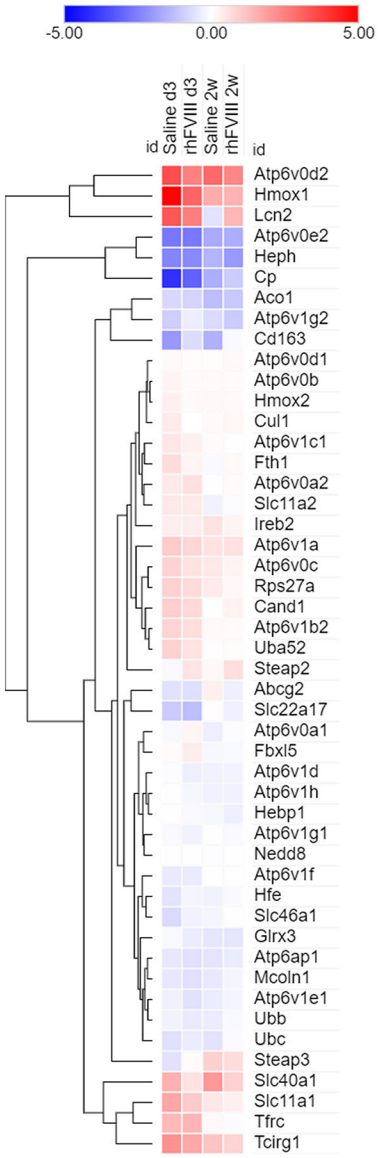

Figure 2. Expression of iron regulators in synovial tissue from FVIII$^{-/-}$ mice after induced hemarthrosis.

Hemarthrosis was induced in FVIII$^{-/-}$ mice by sub-patellar needle puncture +/− peri-procedural recombinant human FVIII (rhFVIII) or saline (vehicle), given 2 hours before and 6 hours after injury (n=3–5 per group). Tissue was harvested at baseline and Day 3 (d3) or 2 weeks (2w) after injury. RNA was purified and analyzed by RNA sequencing using an Illumina NextSeq500 platform (75bp; single-end). The heat map was generated using Morpheus and displays the $\log_2$ fold-change over baseline values for genes related to iron uptake and transport (Reactome pathway) on a color scale from −5 to +5. Rows were clustered using the Euclidian distance method.

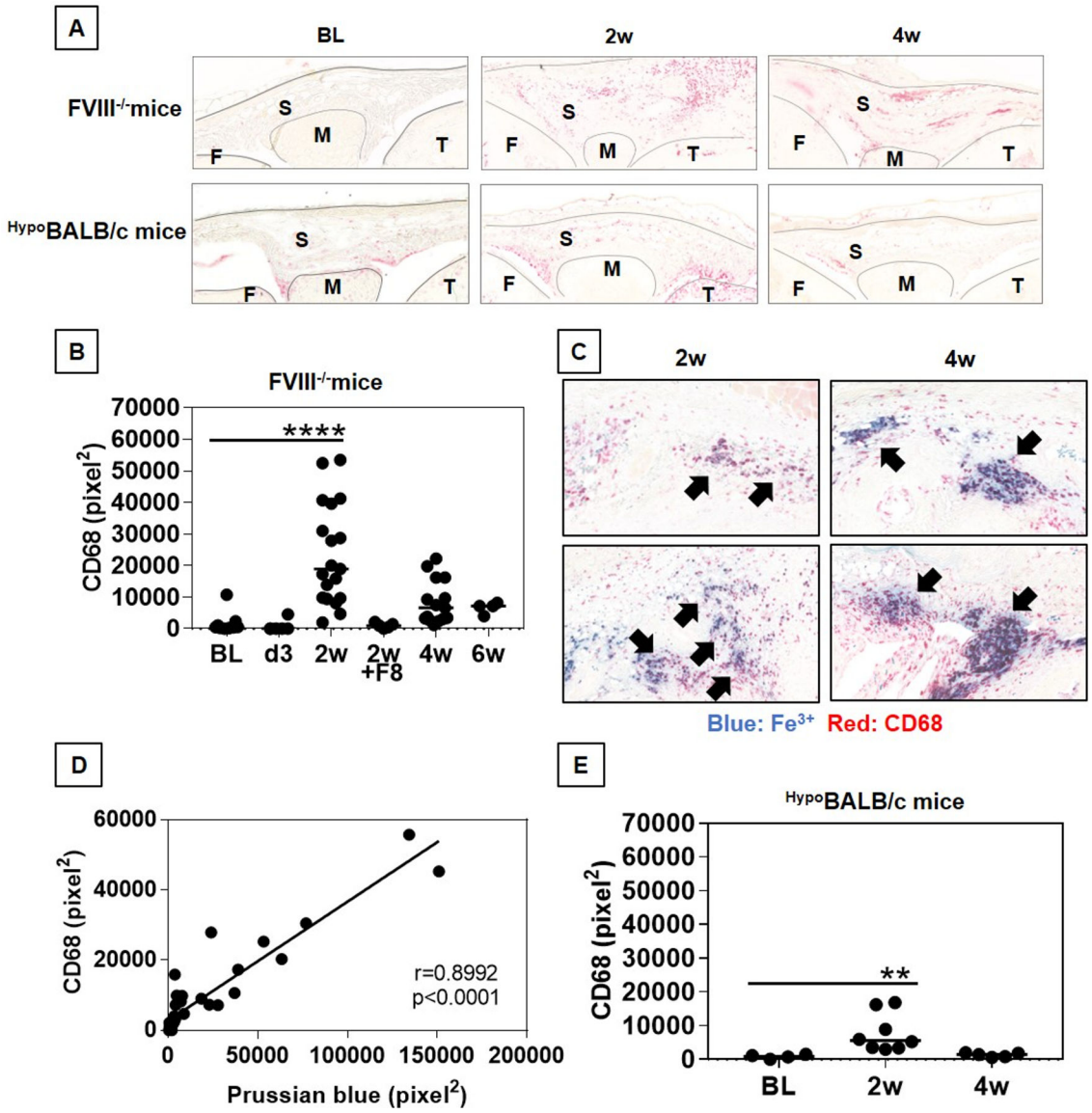

Figure 3. CD68 expression in synovial tissue after induced hemarthrosis.

Joint tissue was harvested from FVIII$^{-/-}$ and ^{Hypo}BALB/c mice at baseline (BL) and 2 weeks (2w), 4 weeks (4w), or 6 weeks (6w) after sub-patellar injury (n=5–19 per group). A group of FVIII$^{-/-}$ mice received peri-procedural recombinant human FVIII with tissue harvest at 2 weeks after injury (2w+F8). Joint tissue was fixed in 10% zinc-buffered formalin, decalcified in 10% (v/v) formic acid containing 0.2% (w/v) potassium ferrocyanide for Perls' Prussian blue staining of ferric iron (Fe^{3+}) (shown in blue) and paraffin-embedded. Tissue sections were subjected to immunohistochemistry with an anti-CD68 antibody (shown in red) and imaged using a Hamamatsu Nanozoomer brightfield slide scanner at 20x magnification. (A) Representative images of synovial CD68 staining in FVIII$^{-/-}$ and ^{Hypo}BALB/c mice, (B/C) quantified using Image J and displayed as median (**p<0.01, ****p<0.0001). (D) Representative images of synovium from FVIII$^{-/-}$ mice at 2 weeks or 4 weeks after hemarthrosis. Black arrows indicate areas of CD68 and Prussian blue

colocalization. (E) Spearman's rank correlation analysis of CD68 and Prussian blue staining (n=35).

F: femur, S: synovium, M: meniscus, T: tibia.

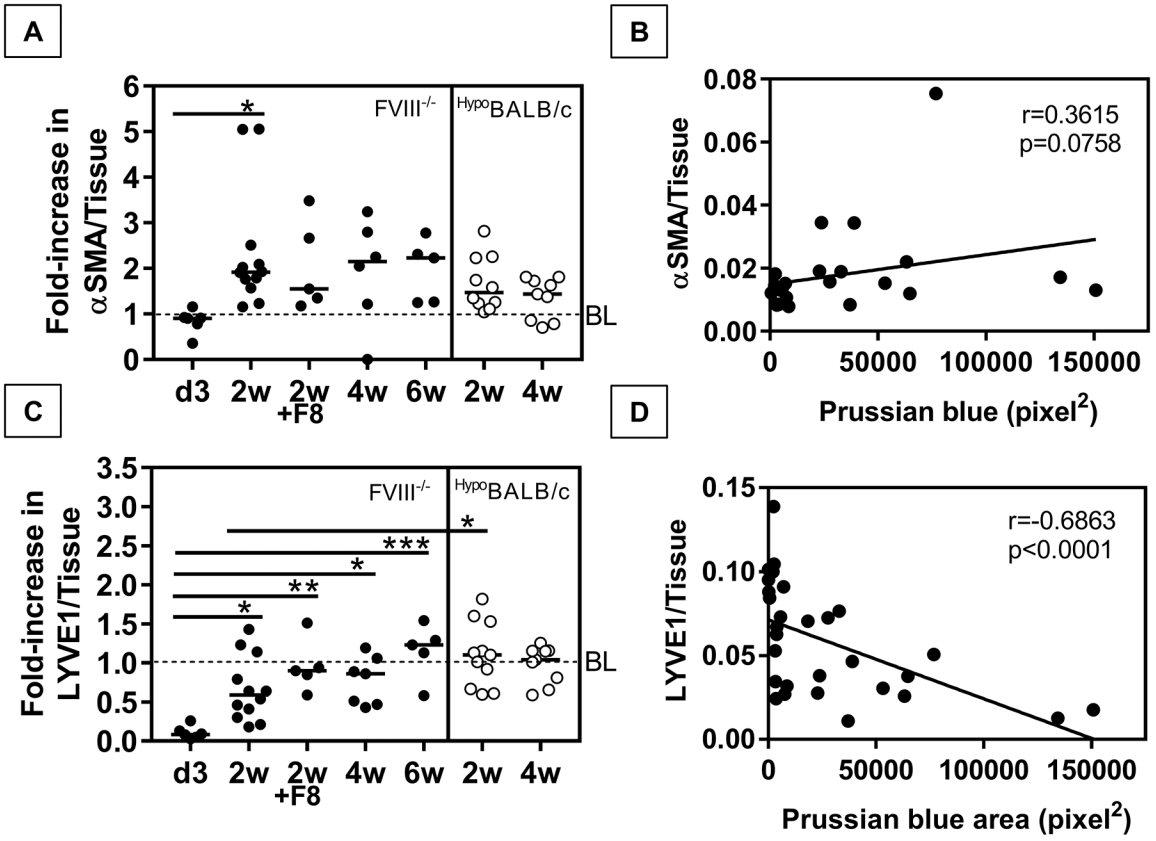

Figure 4. Blood and lymphatic vessel density in synovial tissue from FVIII$^{-/-}$ mice after hemarthrosis.

Joint tissue was harvested from FVIII$^{-/-}$ and HypoBALB/c at baseline (BL), Day 3 (d3), 2 weeks (2w) +/− recombinant human FVIII (F8) peri-procedural treatment, 4 weeks (4w), or 6 weeks (6w) after injury to induce joint bleeding (n=5–12 per group). Immunohistochemistry was performed with an anti-αSMA antibody to detect remodeling blood vessels (A) or an anti-LYVE1 antibody to detect lymphatic vessels (C). Tissue sections were imaged using a Hamamatsu Nanozoomer brightfield slide scanner at 20x magnification and staining was quantified with ImageJ. Stained areas were normalized to tissue area and data in (A) and (C) are displayed as the fold increase over the median baseline value for FVIII$^{-/-}$ or ^{Hypo}BALB/c mice. Error bars represent median values (*p<0.05, **p<0.01, ***p<0.001). Spearman's rank correlation analysis was used to assess relationships in FVIII-deficient mice between Prussian blue staining at 2 to 6 weeks after injury and (B) αSMA normalized to tissue area (n=25) or (D) LYVE1 normalized to tissue area (n=30).

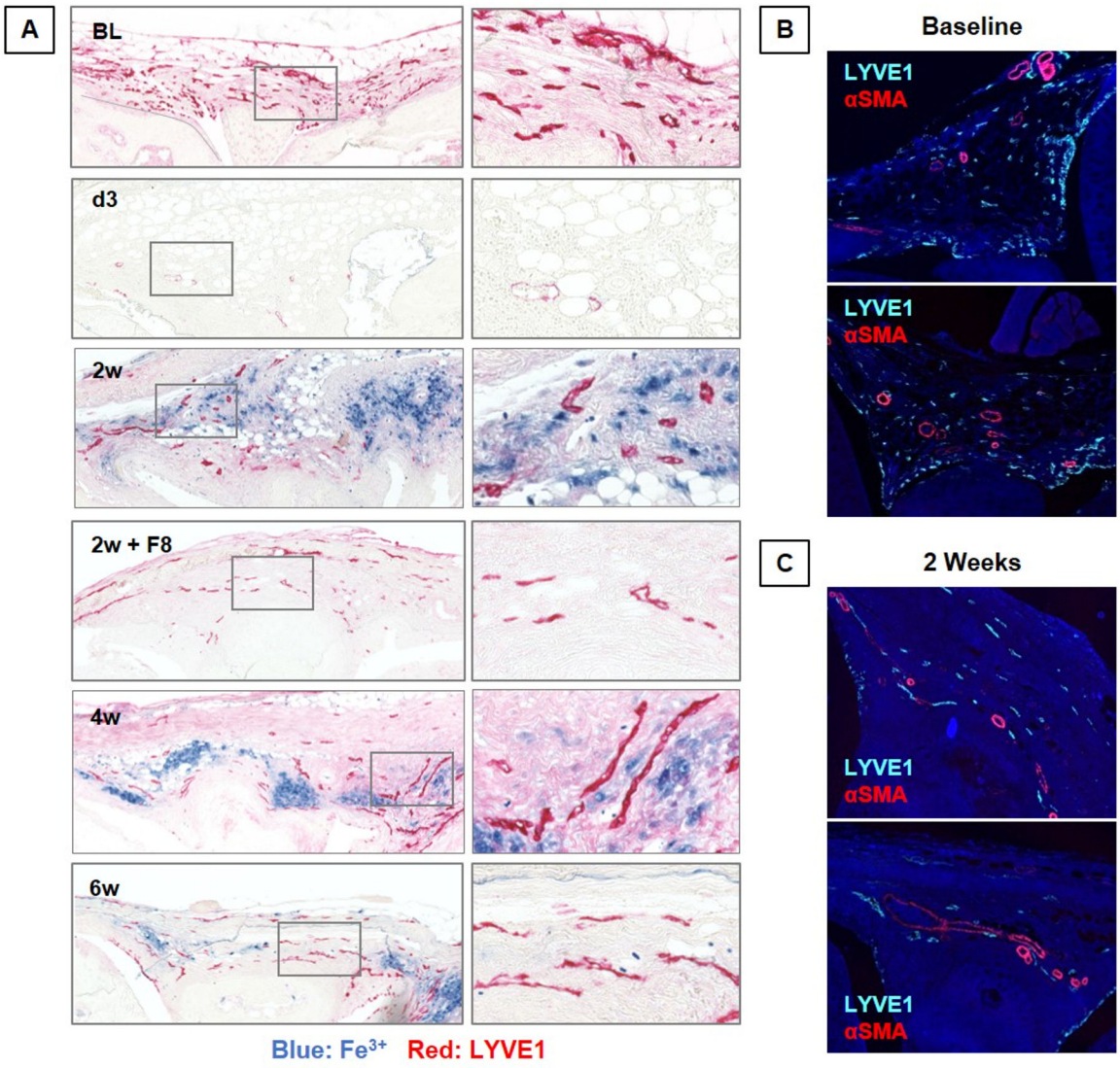

Figure 5. Lymphatic vessels in synovial tissue from FVII$^{I-/-}$ mice after induced joint bleeding.

FVIII$^{-/-}$ mice were subjected to sub-patellar puncture to induce hemarthrosis and joint tissue was harvested at baseline (BL) and Day 3, 2 weeks (2w), 4 weeks (4w), or 6 weeks (6w) after injury. (A) Joints were fixed in 10% zinc-buffered formalin and decalcified in 10% (v/v) formic acid containing 0.2% (w/v) potassium ferrocyanide for Perls' Prussian blue staining of ferric iron (Fe^{3+}) (shown in blue). Tissue sections were subjected to immunohistochemistry with an anti-LYVE1 antibody (shown in red) and imaged using a Hamamatsu Nanozoomer brightfield slide scanner at 20x magnification. (B) and (C) Joints were fixed in 10% zinc-buffered formalin and decalcified in 10 % (v/v) formic acid. Immunofluorescence was performed with anti-LYVE1 (shown in light blue) and anti-αSMA antibodies (shown in red) and tissue sections were imaged by laser scanning confocal microscopy (Zeiss LSM 880) at 10x magnification. Representative examples of baseline (B) and injured mice (C) (2 weeks) are displayed.

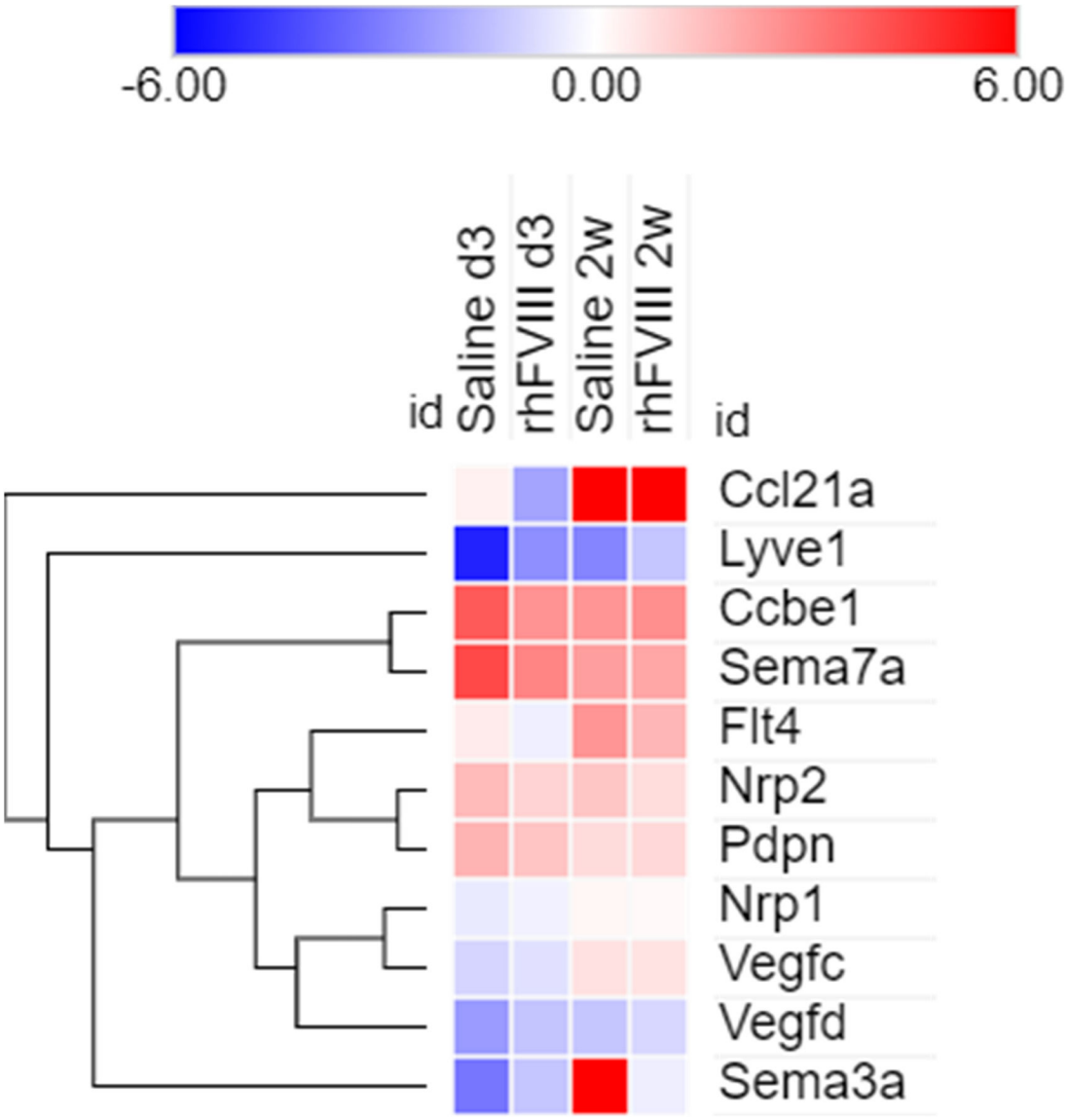

Figure 6. Differential expression of lymphatic markers in synovial tissue from FVIII$^{-/-}$ mice after induced hemarthrosis.

Hemarthrosis was induced in FVIII$^{-/-}$ mice by subpatellar needle puncture +/− peri-procedural recombinant human FVIII (rhFVIII) or saline (vehicle), given 2 hours before and 6 hours after injury (n=3–5 per group). Tissue was harvested at baseline and Day 3 (d3) or 2 weeks (2w) after injury. RNA was purified and analyzed by RNA sequencing using an Illumina NextSeq500 platform (75bp; single-end). The heat map was generated using Morpheus and displays the $\log_2$ fold-change over baseline values for genes related to lymphatic homeostasis on a color scale from −5 to +5. Rows were clustered using the Euclidian distance method.

Table 1.

Differentially expressed markers of iron regulators in synovial tissue from FVIII$^{-/-}$ mice after hemarthrosis.

Synovial tissue was harvested from FVIII$^{-/-}$ mice at baseline and Day 3 or 2 weeks after induced hemarthrosis +/− peri-procedural recombinant human FVIII (rhFVIII) (n=3–5 per group). RNA was purified and analyzed by RNA sequencing using an Illumina NextSeq500 platform (75bp; single-end). Differential expression was determined as $\log_2$ fold-change > 1 or < −1 and $p < 0.05$. The table lists up- (↑) and down-regulated (↓) genes in the Reactome iron uptake and transport pathway, as well as their functions and absolute fold-change at Day 3 or 2 weeks. ND: No significant difference. V-ATPase: vacuolar-type ATPase.

Gene	Protein	Function	Fold-change day 3		Fold-change 2 weeks	
			Saline	rhFVIII	Saline	rhFVIII
Hmox1	Heme-oxygenase-1	Heme-degrading enzyme	31-fold ↑	8-fold ↑	3-fold ↑	3-fold ↑
Atp6v0d2	V-ATPase subunit D 2	Acidification of endosomes; (facilitates iron release from transferrin and transferrin receptor recycling)	11-fold ↑	6-fold ↑	8-fold ↑	5-fold ↑
Lcn2	Lipocalin-2	Iron-binding protein	10-fold ↑	6-fold ↑	ND	ND
Slc11a1	Solute carrier family 11 member 1	Macrophage iron transporter	3-fold ↑	2-fold ↑	ND	ND
Tfrc	Transferrin receptor	Endocytosis of (iron-bound) transferrin	3-fold ↑	3-fold ↑	ND	ND
Atp6v1a	V-ATPase catalytic subunit A	Acidification of endosomes (facilitates iron release from transferrin and transferrin receptor recycling)	2-fold ↑	ND	ND	ND
Cp	Ceruloplasmin	Ferroxidase; efflux of cellular iron	17-fold ↓	8-fold ↓	3-fold ↓	ND
Atp6v0e2	V-ATPase subunit E 2	Acidification of endosomes (facilitates iron release from transferrin and transferrin receptor recycling)	6-fold ↓	6-fold ↓	3-fold ↓	3-fold ↓
Heph	Hephaestin	Ferroxidase; efflux of cellular iron	5-fold ↓	5-fold ↓	3-fold ↓	4-fold ↓
Cd163	Cluster of differentiation 163	Hemoglobin scavenging receptor (macrophages)	5-fold ↓	ND	3-fold ↓	ND
Aco1	Acotinase 1	Transcriptional regulation of intracellular iron	ND	ND	2-fold ↓	2-fold ↓
Slc22a17	Solute carrier family 22 member 17	Lipocalin-2 receptor	2-fold ↓	2-fold ↓	ND	ND
Atp6v1g2	V-ATPase subunit G 2	Acidification of endosomes (facilitates iron release from transferrin and transferrin receptor recycling)	ND	ND	ND	2-fold ↓

Table 2.

Differentially expressed markers of lymphatic vessels and remodeling in synovial tissue from FVIII$^{-/-}$ mice after hemarthrosis.

Synovial tissue was harvested from FVIII$^{-/-}$ mice at baseline and Day 3 or 2 weeks after induced hemarthrosis +/− peri-procedural recombinant human FVIII (rhFVIII) (n=3–5 per group). RNA was purified and analyzed by RNA sequencing using an Illumina NextSeq500 platform (75bp; single-end). Differential expression was determined as $\log_2$ fold-change > 1 or < −1 and $p < 0.05$. The table lists absolute fold-change values for up- (↑) and down-regulated (↓) genes. ND: No significant difference. LEC: lymphatic endothelial cell, CCR7: C-C motif chemokine receptor 7, DC; dendritic cell, VEGF(R): vascular endothelial growth factor (receptor), EGF: epidermal growth factor.

Gene	Protein	Function	Fold-change day 3		Fold-change 2 weeks	
			Saline	rhFVIII	Saline	rhFVIII
Ccl21a	Chemokine (C-C motif) ligand 21	Constitutively expressed by LECs; prominent role in trafficking CCR7+ cells through lymphatic vessels	ND	ND	194-fold ↑	79-fold ↑
Sema7a	Semaphorin 7a	Drives podoplanin-dependent adherence of macrophages and DCs to LECs to promote lymphangiogenesis; regulates CCL21-mediated migration of DCs	20-fold ↑	7-fold ↑	5-fold ↑	ND
Ccbe1	Collagen and calcium binding EGF domains 1	Required for budding and maturation of LECs; enhances the lymphangiogenic effect of VEGF-C	15-fold ↑	6-fold ↑	6-fold ↑	7-fold ↑
Flt4	FMS-like tyrosine kinase 4 (VEGFR3)	Receptor for VEGF-C and VEGF-D on LECs	ND	ND	6-fold ↑	3-fold ↑
Nrp1	Neuropilin 1	Receptor for Sema3a and isoform of $Vegf_{165}$; regulates vessel maturation, enhances cell migration during angiogenesis	1-fold ↓	1-fold ↓	1-fold ↑	1-fold ↑
Nrp2	Neuropilin 2	Receptor for VEGF-C; mediates VEGF-C-induced lymphatic sprouting	3-fold ↑	2-fold ↑	2-fold ↑	ND
Pdpn	Podoplanin	Expressed in LECs; function unknown	3-fold ↑	3-fold ↑	ND	ND
Lyve1	Lymphatic vessel endothelial hyaluronan receptor 1	Hyaluronic acid receptor expressed on LECs; plays a role in dendritic cell docking	37-fold ↓	6-fold ↓	7-fold ↓	3-fold ↓
Sema3a	Semaphorin 3a	Expressed in LECs; binds neuropilin-1 to facilitate lymphatic valve formation and entry of dendritic cells into lymphatic vessels	9-fold ↓	3-fold ↓	2-fold ↓	ND
Vegfd	Vascular endothelial growth factor D	Lymphangiogenic factor; regulates proliferation and migration of LECs via VEGFR	5-fold ↓	3-fold ↓	2-fold ↓	ND
Vegfc	Vascular endothelial growth factor C	Lymphangiogenic factor; principle driver of lymphangiogenesis	2-fold ↓	2-fold ↑	2-fold ↑	2-fold ↑
Sema3d	Semaphorin 3d	Expressed in LECs; binds neuropilin-1 to regulate actin network organization and stabilizes EC sheet	9-fold ↓	3-fold ↓	1-fold ↓	1-fold ↓